Research Article

Competitive Adsorption as a Route to Area-Selective Deposition

Taewon Suh, Yan Yang, Pengyuan Zhao, Ka Un Lao, Hsin-Yu Ko, Jonathan Wong, Robert A. DiStasio, Jr.,* and James R. Engstrom*

Cite This: https://dx.doi.org/10.1021/acsami.9b22065

Read Online

ACCESS | Metrics & More | Article Recommendations | SI Supporting Information

ABSTRACT: In this work, we have explored the use of a third species during chemical vapor deposition (CVD) to direct thin-film growth to occur exclusively on one surface in the presence of another. Using a combination of density functional theory (DFT) calculations and experiments, including in situ surface analysis, we have examined the use of 4-octyne as a coadsorbate in the CVD of ZrO_2 thin films on SiO_2 and Cu surfaces. At sufficiently high partial pressures of the coadsorbate and sufficiently low substrate temperatures, we find that 4-octyne can effectively compete for adsorption sites, blocking chemisorption of the thin-film precursor, $Zr[N(CH_3C_2H_5)]_4$, and preventing growth on Cu, while leaving growth unimpeded on SiO_2. The selective dielectric-on-dielectric (DoD) process developed herein is fast, totally vapor phase, and does not negatively alter the composition or morphology of the deposited thin film. We argue that this approach to area-selective deposition (ASD) should be widely applicable, provided that suitable candidates for preferential binding can be identified.

KEYWORDS: area-selective deposition (ASD), chemical vapor deposition (CVD), competitive adsorption, coadsorbate, 4-octyne, dielectric-on-dielectric (DoD), density functional theory (DFT), binding free energies
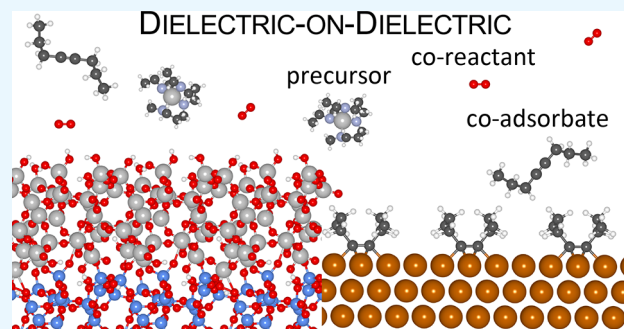
INTRODUCTION

Spatial control of chemical reactions occurring on solid surfaces at atomic and molecular dimensions is important to a variety of technologies ranging from catalysis and sensing, to thin-film processes such as deposition, patterning, and etching.[1,2] Concerning the latter, a significant challenge for single-nm fabrication technologies is the development of area-selective deposition (ASD) processes, particularly for device structures with exposed metallic, dielectric, and semiconductor surfaces on patterned (and often three-dimensional) substrates. Self-aligned ASD processes, in particular, also require that the deposition process exhibits a dependence on substrate composition, involving a growth and nongrowth surface. Successful ASD processes have been demonstrated for some time using chemical vapor deposition (CVD),[3−7] and more recently using atomic layer deposition (ALD).[8−12] For each deposition technique, there are several successful examples representing different material systems, as well as different approaches to achieve selectivity. One distinguishing factor concerning growth via CVD vs ALD is that the former is often conducted at relatively high temperatures where the reversibility of adsorption can be exploited. ALD, however, involves sequential half-reactions that proceed to completion irreversibly.[13−15]

Concerning AS-ALD, achieving selectivity typically focuses on preventing the irreversible chemisorption of the thin-film precursor, 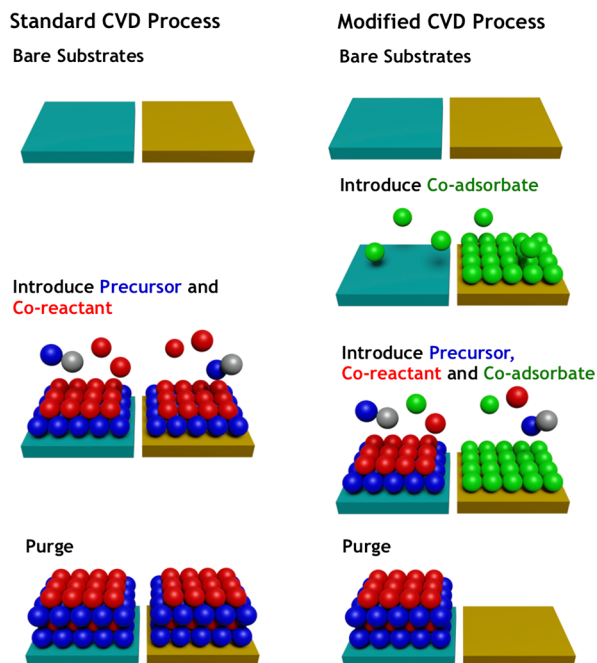often a transition metal coordination complex or a main group compound, on the nongrowth surface where growth is not desired. In some cases, the inherent reactivity of the thin-film precursor with the surface is low enough that the growth is sufficiently delayed (i.e., nucleation delay) such that finite selectivity can be achieved. There are also examples where the reactivity differences are due to the chemical identity of the surface[16,17] or the ALD chemistry (i.e., precursor and coreactant) itself.[18] Another method that has been explored involves "reversing" chemisorption of the precursor by introducing an "etch-back" step,[19−21] which possesses several similarities to the reversibility exploited in some AS-CVD processes. Perhaps the most examined approach in AS-ALD to date involves the use of blocking layers in the form of self-assembled monolayers (SAMs).[8,9,22,23] While this approach has its merits, it often suffers from very slow solution-phase formation of the SAMs, degradation over time and exposure to the coreactant (catastrophic with exposure to a plasma), and undesirable effects of surface topography where blocking effects break down.[24]

In this work, we explore an alternative strategy that involves the introduction of a third chemical species (referred to as the

coadsorbate), that primarily competes with the thin-film precursor (and potentially the coreactant species) for surface binding sites. We display this process schematically in Figure 1,

Standard CVD Process
Bare Substrates

Introduce Precursor and Co-reactant

Purge

Modified CVD Process
Bare Substrates

Introduce Co-adsorbate

Introduce Precursor, Co-reactant and Co-adsorbate

Purge

Figure 1. Schematic representing the process flow for CVD thin-film growth on one surface (teal) vs another (gold), due to the introduction of a coadsorbate species (green), in addition to the thin-film precursor (blue) and the coreactant (red). The coadsorbate is selected to bind much more strongly to the nongrowth surface, such that it builds up a high coverage and effectively blocks CVD growth.

where two substrate surfaces are subjected to a modified CVD process. First, a *properly selected* coadsorbate species is introduced that binds preferentially to the nongrowth surface, but does not bind sufficiently strongly to the growth surface. Second, the thin-film precursor and coreactant are introduced, and the continued presence of the coadsorbate maintains a high surface coverage to block growth on the nongrowth surface while not impacting growth on the desired growth surface. Finally, after all species have been purged from the gas phase, the coadsorbate can desorb leaving the nongrowth surface essentially untouched.

Importantly, our concept can be applied to both ALD and CVD processes; in an ALD process, one might choose to introduce the coadsorbate during the thin-film precursor half-cycle only. We note that our approach has some similarities to approaches investigated by others. For example, repetitive introduction of a third species in a so-called "ABC" type ALD process has produced some success concerning the selective growth of SiO₂ on a range of main group and transition metal oxide surfaces.[25] Use of a molecular inhibitor has also been investigated in single-source (no coreactant) CVD of Cu[26] and transition metal oxide and oxy-nitride thin films.[27] However, these prior studies lack several important features of our approach. First, coflow of the thin-film precursor and the coadsorbate is intentional on our part in order to exploit the effects of competitive adsorption,[28] where chemisorption of the coadsorbate can be *reversible* on the nongrowth surface (see Figure 1). Reversible adsorption in this case alleviates the need for additional postdeposition processing on the nongrowth

surface. Second, we include a coreactant in our process, which is obviously required for any ALD process and most CVD processes. Third, our approach involves entirely vapor-phase species, which is highly desirable for high volume manufacturing, and holds promise for plasma-based ALD, since the coadsorbate exposure coincides with the thin-film precursor (and not the coreactant) half-cycle.

As a specific example of this approach, we report here on a robust CVD process in which ZrO₂ thin films are selectively grown on SiO₂ in the presence of Cu. In particular, we demonstrate how this dielectric-on-dielectric (DoD) growth process can be accomplished using tetrakis(ethylmethylamido) zirconium (TEMAZ), $Zr[N(CH_3C_2H_5)]_4$, as the thin-film precursor, O₂ as the coreactant, and 4-octyne as the coadsorbate species. On the basis of dispersion-inclusive density functional theory (DFT) calculations, we show that the binding of 4-octyne is significantly different on these two surfaces, which facilitates selective blocking of deposition on the nongrowth surface (Cu), while having minimal impact on deposition on the growth surface (SiO₂). By exploring how the selectivity depends on the substrate temperature and partial pressure (of the coadsorbate), we demonstrate that our approach is consistent with a simple site-blocking mechanism and competitive adsorption.

EXPERIMENTAL AND THEORETICAL PROCEDURES

Experiments. The experiments described herein were conducted in a custom-designed, multiple-stage stainless steel UHV chamber, which we have described in detail previously.[29,30] This system consists of a source and antechamber used to generate supersonic molecular beams (not employed here), a main surface analysis chamber, an intermediate chamber, and a fast entry load-lock chamber. The main analysis chamber (base pressure of ~9 × 10⁻¹⁰ Torr) houses a concentric hemispherical electron energy analyzer and a twin anode Mg/Al X-ray source that are employed for X-ray photoelectron spectroscopy (XPS).[31] The substrates are mounted on a precision sample manipulator (x–y–z and polar and azimuthal angles), and translation along the long axis of the manipulator takes the samples to and from the intermediate and main analysis chambers. The substrates are heated radiatively by a pyrolytic boron nitride heating element that is incorporated in the manipulator. Once inside the intermediate chamber, the manipulator and substrates are isolated from the main analysis chamber, and samples can be loaded using a magnetically coupled transfer arm mounted to the load-lock.

In the intermediate chamber, a reaction zone is formed by the sample holder and a custom-designed probe mounted to a translation stage that both delivers the gas-phase reactants to the sample surface, and pumps the products away.[32] For the experiments conducted in this work, we employed a custom-made substrate platen designed to hold two coupon size samples (ca. 9 × 29 mm²), enabling study of a deposition process on two different samples under identical conditions. After thin-film deposition and (typically) in situ analysis using XPS without air-break, a number of ex situ analyses were also conducted including spectroscopic ellipsometry (SE, Woollam) and atomic force microscopy (AFM, Bruker Innova, tapping mode).

The substrates used here were Si wafers of two types. In one case, samples were cleaved (i.e., scribed and diced) from double-side polished Si(100) wafers (B doped, resistivity 38–63 Ω cm), and then the native SiO₂ layer was removed from the substrates by dipping in buffered oxide etch (BOE) for 2 min. The substrates were then reoxidized by dipping in Nanostrip for 15 min at a temperature of ~75 °C. The BOE/Nanostrip treatment was then repeated. This method is known to produce a 15–20 Å layer of SiO₂ ("chemical oxide"). In a second case, Si wafers with a 100 nm thick film of PVD Cu|Ta(adhesion layer)|SiO₂ were cleaved into coupon sized samples and then used as-received.

The thin-film precursor, $Zr[N(CH_3C_2H_5)]_4$ (TEMAZ, Air Liquide, 99.99%), was delivered to the substrate by flowing a carrier gas (N_2, Airgas, UHP) regulated by a mass-flow controller (MFC) through a stainless steel bubbler. The partial pressure of the thin-film precursor reaching the substrate was determined by controlling the temperature of the stainless steel bubbler. The O_2 (Airgas, UHP) was delivered to the substrate directly from a high-pressure gas cylinder using a MFC. Finally, the 4-octyne (Sigma-Aldrich, 99%) was delivered to the substrate by flowing a carrier gas (N_2, Airgas, UHP) regulated by a MFC through a stainless steel bubbler (kept at a constant temperature). The partial pressure of the 4-octyne reaching the substrate was determined by controlling the fraction of carrier gas that flowed directly through the stainless steel bubbler vs that flowing through a parallel line that bypassed the bubbler. Four independently controlled streams enter the reaction zone: thin-film precursor, coreactant, coadsorbate, and a "curtain" gas.[32] In the absence of a reactant flow, an equivalent amount of inert purge gas was allowed to flow through each line (controlled by fast acting solenoid valves) such that the total gas flow rate remained constant during the course of an experiment. The total pressure in the reaction zone is regulated by a throttle valve on the exit stream of the microreactor. The total pressure for all thin-film deposition experiments was 1.5 Torr, and the residence time for the reactants in the reaction zone for the conditions examined here was 3.9−5.1 ms.

Theoretical Calculations. In this work, we simulated the electronic structure of all systems using periodic Kohn−Sham density functional theory (KS-DFT) in the planewave and psudopotential-based Quantum ESPRESSO (QE) program.[33] The electronic exchange-correlation (XC) energy was modeled using the Perdew−Burke−Ernzerhof (PBE)[34] generalized-gradient approximation (GGA) supplemented with a self-consistent implementation[35] of the effective-pairwise Tkatechenko-Scheffler (TS)[36] van der Waals/dispersion (vdW) correction, which has been modified to account for molecule−surface vdW interactions (vdW^{surf}).[37] In this work, we utilized vdW parameters from previous work for the following elements: Si and O,[38] H and C,[36] and Cu.[37] For each atomic species, the core electrons were modeled using Hamann-Schlüter-Chiang-Vanderbilt (HSCV) norm-conserving pseudopotentials,[39,40] with the exception of Cu, whose pseudopotential was constructed via the optimized norm-conserving Vanderbilt (ONCV) approach.[41] The valence (pseudo)wave functions were represented explicitly in a planewave basis with a kinetic energy cutoff of 85 Ry. During each self-consistent field (SCF) calculation, we converged the total electronic energy (U^{DFT}) to <10^{-10} Ry. During structural (geometry) optimizations, the Broyden-Fletcher-Goldfarb-Shanno (BFGS) algorithm was used to relax the ionic positions such that variations in U^{DFT} between BFGS steps were <10^{-6} Ry, and the maximum ionic force was <10^{-4} Ry/Bohr. During variable-cell (VC) optimizations, the BFGS algorithm was also used to relax the cell tensor such that the total internal pressure was <0.5 kBar.

For the copper (Cu) surface, we performed an initial VC optimization of bulk Cu in a cubic cell containing 32 atoms at the PBE+vdW^{surf} level of theory, in which the ionic and cell degrees of freedom were relaxed. In this case, the first Brilluoin zone (FBZ) was sampled using an $8 \times 8 \times 8$ k-point mesh (via the Monkhorst−Pack approach).[42] This optimized unit cell (with lattice parameter $a = 3.58$ Å) was then used to generate metallic slabs (each of which contained six Cu layers) as models for the high-symmetry/low-index Cu(111), Cu(110), and Cu(100) surfaces. To reduce the spurious interactions with vertical periodic images, we introduced an ~20 Å vacuum region along the surface normal direction in each unit cell. In doing so, we obtained the following orthorhombic simulation cells: $8.72 \times 10.12 \times 30.00$ Å^3 for Cu(111) containing 96 atoms; $10.12 \times 10.74 \times 30.00$ Å^3 for Cu(110) containing 72 atoms; $10.74 \times 10.74 \times 30.00$ Å^3 for Cu(100) containing 108 atoms. During the structural optimization of each Cu substrate (**S**) and Cu substrate + adsorbate (**S+A**) system, the ionic positions of the top two Cu layers were relaxed while the bottom four layers were kept fixed (constrained), and the FBZ was sampled using a $2 \times 2 \times 1$ k-point mesh. For the isolated adsorbate (**A**), structural optimizations were carried out in the same cell as

S and **S+A**, and the FBZ was sampled at the Γ-point only. In all calculations on the **A** and **S+A** systems, the vdW interactions between **A** and its periodic images were switched off, thereby allowing us to model the interaction between a single adsorbate and the underlying substrate. To obtain the final value for U^{DFT}, single-point SCF calculations were performed using a $4 \times 4 \times 1$ k-point mesh for the optimized **S** and **S+A** systems, while the Γ-point was again used for the optimized **A** system.

For the hydroxyl-terminated silica (SiO$_2$) surface, we built an amorphous 99-atom model system[43] (Si$_{27}$O$_{60}$H$_{12}$) with a hydroxyl (−OH) surface density of 5.07 nm^{-2}; in a $10.72 \times 11.03 \times 30.00$ Å^3 orthorhombic simulation cell, our model contains six unique −OH sites (which includes vicinal and geminal −OH moieties). During the structural optimization of the SiO$_2$ substrate (**S**), we relaxed the ionic positions at the PBE+vdW^{surf} level, while maintaining the original constraints for the atoms in the bulk region.[43] Subsequent structural optimizations of the corresponding **A** and **S+A** systems were carried out in the same unit cell. During all calculations on these systems, the FBZ was sampled at the Γ-point only (which is converged with respect to k-point sampling). To model the interaction between a single adsorbate and the underlying silica substrate, the vdW interactions between **A** and its periodic images were again switched off during all calculations on the **A** and **S+A** systems.

All phonon frequencies were numerically computed in the harmonic approximation using the PHONOPY package.[44] Perturbed geometries were constructed from the relaxed (optimized) geometries described above using a finite-difference step size of 0.005 Å. In the SCF calculation for each perturbed geometry, we converged U^{DFT} to <10^{-12} Ry in QE (a more stringent convergence criterion to reduce the numerical error in the phonon frequencies). As some of the substrate atoms were fixed during the structural optimizations of the **S** and **S+A** systems, the same sets of constraints were applied during the phonon calculations. In particular, this was done by assigning an infinitely large mass to the frozen/constrained atoms when forming the mass-weighted dynamical (Hessian) matrix, such that the resulting sub-blocks involving these atoms were set to zero. Since the constrained **S** and **S+A** systems are not translationally or rotationally invariant, all $3N$ degrees of freedom (with N equal to the number of *unconstrained* atoms) were considered when computing the vibrational contributions to the binding energies. For the isolated **A** systems, the translational and rotational contributions to the binding energies were treated in the ideal gas (IG) and rigid rotor (RR) approximations, respectively. As such, these degrees of freedom were projected out of the mass-weighted dynamical (Hessian) matrix before diagonalization,[45] thereby resulting in $3N$-6 degrees of freedom in the vibrational contributions to the binding energies.

Electronic binding energies (ΔU^{DFT}), binding enthalpies [$\Delta H(T,p)$], and binding Gibbs free energies [$\Delta G(T,p)$] were computed via the following:

$$\Delta U^{DFT} = U_{S+A}^{DFT} - U_S^{DFT} - U_A^{DFT} \qquad (1)$$

$$\Delta H(T, p) = H_{S+A}(T, p) - H_S(T, p) - H_A(T, p) \qquad (2)$$

$$\Delta G(T, p) = G_{S+A}(T, p) - G_S(T, p) - G_A(T, p) \qquad (3)$$

using a substrate temperature of $T = T_s = 120$ °C and a partial pressure of $p = p_A = 0.36$ Torr. For a detailed description of the procedure used to compute eqs 1−3, see the *Binding Energetics* section of the Supporting Information (SI).

Theoretical Expectations. In the approach described herein, we intentionally added a third species into our process as shown in Figure 1, which introduces additional interactions into conventional ALD or CVD chemistries. In Figure 2, we display some of these interactions that one must consider in this approach, with a primary focus on those involving the thin-film precursor and the coadsorbate species. As may be seen in this schematic, there are at least five interactions to consider and optimize. For any deposition process, efficient nucleation requires strong interaction/high reactivity between the thin-film precursor and the desired growth surface. In some cases, large enough differences in reactivity between surfaces are sufficient to
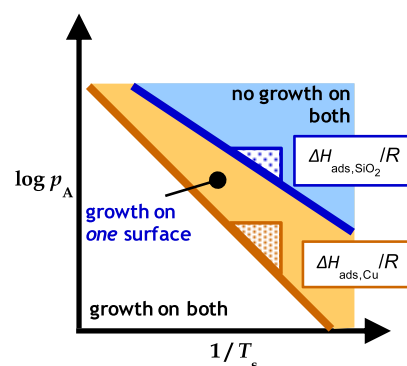
Figure 2. Schematic representing the interactions that must be considered when employing a coadsorbate to achieve area-selective deposition (ASD). This does not include the additional interactions (as many as four) that are also introduced in a CVD process by the coreactant.

Figure 3. Schematic representing the process phase space plotted in terms of the logarithm of the partial pressure of the coadsorbate (log p_A) and the inverse temperature ($1/T_s$). The straight lines represent constant coverages that would be sufficient (e.g., $\theta_c \approx 0.999$) to block thin-film growth/dissociative chemisorption of the thin-film precursor. In this simple model, we assume that a Langmuir isotherm applies to both surfaces, and the chosen coadsorbate binds more strongly to the metal (Cu) vs the dielectric (SiO$_2$) surface.

Nevertheless, this analysis makes the important point that the partial pressure of the coadsorbate and the substrate temperature are the two key process variables governing selectivity in our approach.

■ RESULTS

Density Functional Theory Calculations. To facilitate the identification of suitable coadsorbate molecules that can direct thin-film growth on the desired growth surface (by preferentially adsorbing onto the nongrowth surface), we conducted a series of dispersion-inclusive DFT calculations to determine the binding energetics associated with the adsorption of candidate coadsorbate molecules onto the SiO$_2$ and Cu surfaces. Previous work has shown the utility of DFT when investigating the mechanisms of thin-film growth including ALD.[46] Here, we summarize a subset of our computational work by focusing on the binding energetics of 4-octyne on these surfaces, which shows great promise as the coadsorbate species in our competitive adsorption approach.

Our first task was to identify the representative binding motifs of 4-octyne, an unsaturated hydrocarbon with an internal alkyne (triple bond) moiety [see Figure 4(a)], on an amorphous hydroxyl-terminated SiO$_2$ surface and the high-symmetry/low-index facets of Cu, i.e., Cu(111), Cu(110), and Cu(100). First, we consider the binding of a single 4-octyne molecule on the SiO$_2$ surface. Since we do not anticipate any low activation barrier routes to a chemisorbed species on SiO$_2$, we expect physisorption of this unsaturated hydrocarbon on the dielectric surface due to nonbonded vdW/dispersion interactions. Here, we note in passing that the treatment of vdW/dispersion interactions in our calculations (via a self-consistent implementation of the vdW^{surf} model[35−37]) utilizes Lifshitz-Zaremba-Kohn (LZK) theory[47,48] to provide an accurate and reliable description of the nonbonded interactions between molecules and surfaces. Since there are no specific binding sites for an alkyne on SiO$_2$, we performed structural optimizations of six randomly chosen initial configurations of the 4-octyne/SiO$_2$ system, and depict the optimized binding motifs for the three most favorable configurations in Figure 4(b). From the corresponding binding energetics provided in Table 1, one sees that the electronic binding energies (ΔU^{DFT}) for 4-octyne on SiO$_2$ are −12.06 kcal-mol^{-1} (Binding Motif #1), −13.71 kcal-mol^{-1} (Binding Motif #2), and −14.96 kcal-

produce an inherent selectivity that may be acceptable for some applications. In our approach, the differential binding of the coadsorbate to the two surfaces must be large. Fortunately, there are a plethora of functional groups and binding motifs that can be considered, which should allow for multiple options concerning the selection of the coadsorbate species. In addition, the interaction between the coadsorbate and the thin-film precursor must also be optimized. To promote competitive adsorption and site-blocking by the coadsorbate, it is often desirable to employ a relatively high partial pressure of the coadsorbate vis-à-vis the thin-film precursor. This could result in undesirable direct interactions in the vapor phase between the coadsorbate and the thin-film precursor via ligand exchange reactions. Hence, the molecular structure of both the coadsorbate and the ligands on the precursor should be chosen to minimize these undesirable interactions.

A simple model can predict the processing landscape that could result in growth on one surface in the presence of another. Let us assume that the coadsorbate binds molecularly and reversibly to the surface, and the Langmuir isotherm model for nondissociative adsorption is applicable (the argument will be similar for reversible dissociative adsorption). On a plot of the logarithm of the adsorbate partial pressure (log p_A) vs inverse temperature ($1/T_s$), theoretical analysis shows that straight lines will be produced that represent constant adsorbate coverage. The slope of these lines represents the quantity $\Delta H_{ads}/R$, in which ΔH_{ads} is the heat (enthalpy) of adsorption and R is the gas constant. If one imagines, for example, that a critical coverage (e.g., θ_c = 0.9, 0.99, 0.999, . . .) exists for chemisorption to be blocked by the coadsorbate, and that this molecule binds differentially to two surfaces, then we are presented with the plot shown in Figure 3. Here the two plotted straight lines would represent this critical coverage (e.g., $\theta_{c,SiO2} = \theta_{c,Cu}$) achieved on the two surfaces. As a result, the following three regions in the processing landscape are predicted to exist: one where growth will occur on both surfaces, one where growth will not occur on both surfaces, and one where growth is selective and will only occur on one surface. This analysis, which assumes equilibrium involving the coadsorbate only, is of course oversimplified and ignores dynamic competition for binding sites, where chemisorption of the thin-film precursor is likely irreversible.
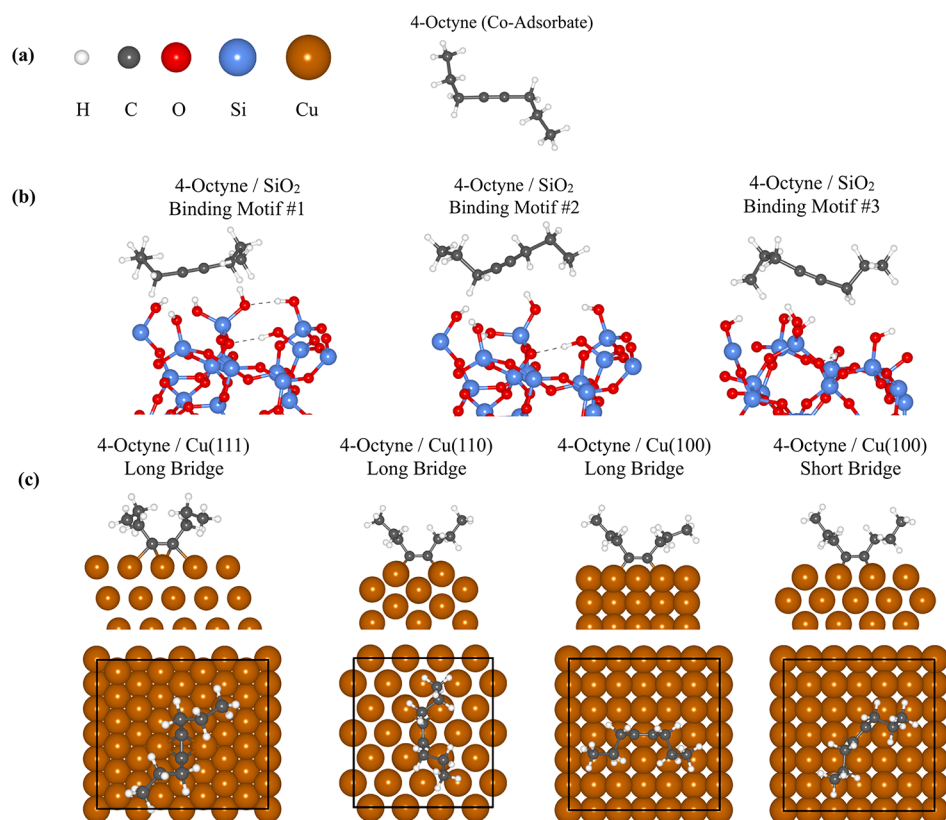
Figure 4. Optimized binding motifs of 4-octyne [vapor-phase molecular structure in panel (a)] on an amorphous hydroxyl-terminated SiO$_2$ surface [side views in panel (b)] and the three high-symmetry/low-index facets of Cu [side and top views in panel (c)]. These panels illustrate that 4-octyne undergoes significant geometrical changes (i.e., $sp \rightarrow sp^2$ rehybridization) upon adsorption to the Cu (and not the SiO$_2$) surfaces.

Table 1. Electronic Binding Energies [ΔU^{DFT}], Binding Enthalpies [$\Delta H(T,p)$], and Binding Gibbs Free Energies [$\Delta G(T,p)$] for the Selected Binding Motifs of 4-Octyne on an Amorphous Hydroxyl-Terminated SiO$_2$ Surface [Figure 4(b)] and the High-Symmetry/Low-Index Facets of Cu [Figure 4(c)][a]

System	ΔU^{DFT} (kcal-mol^{-1})	ΔH (kcal-mol^{-1})	ΔG (kcal-mol^{-1})	C≡C (Å)	C−C≡C (°)
4-octyne	-	-	-	1.21	178.8
SiO$_2$ (Binding Motif #1)	-12.06	-11.28	15.79	1.22	177.6
SiO$_2$ (Binding Motif #2)	-13.71	-12.25	10.89	1.22	175.4
SiO$_2$ (Binding Motif #3)	-14.96	-15.13	16.76	1.20	174.4
Mean (SiO$_2$)	**-13.58 ± 1.45**	**-12.89 ± 2.00**	**14.48 ± 3.15**	**1.21 ± 0.01**	**175.8 ± 1.6**
Cu(111) Long Bridge	-39.70	-39.84	-5.92	1.37	126.5
Cu(110) Long Bridge	-35.68	-37.21	-2.88	1.38	123.0
Cu(100) Long Bridge	-42.06	-42.85	-12.46	1.37	125.8
Cu(100) Short Bridge	-41.19	-42.02	-11.23	1.38	124.1
Mean (Cu)	**-39.66 ± 2.83**	**-40.48 ± 2.52**	**-8.12 ± 4.50**	**1.38 ± 0.01**	**124.9 ± 1.6**

[a]Finite temperature (T) and pressure (p) effects were computed using a substrate temperature of $T = T_s = 120$ °C and a partial pressure of 4-octyne of $p = p_A = 0.36$ Torr. Corresponding C≡C bond lengths (in Å) and averaged C−C≡C (and C≡C−C) bond angles (in °) are also presented for the isolated and surface-bound 4-octyne, demonstrating that this molecule undergoes significant geometrical changes upon adsorption to the Cu (and not the SiO$_2$) surfaces. These changes are indicative of a rehybridization ($sp \rightarrow sp^2$) of the alkyne moiety in 4-octyne, and lead to substantially more favorable binding energetics on the metal surface.

mol^{-1} (Binding Motif #3). With a mean value of $\Delta U^{\mathrm{DFT}} = -13.58 \pm 1.45$ kcal-mol^{-1}, these binding energetics are consistent with physisorption of the coadsorbate molecule onto the dielectric surface.

On the Cu surface, the adsorption of 4-octyne is quite different. In this case, we note that alkynes (e.g., acetylene) are

known to undergo rehybridization ($sp \rightarrow sp^2$) upon binding to Cu surfaces,[49] which results in substantially more favorable binding energetics than one would expect from vdW/dispersion interactions alone. In this work, we considered three distinct binding sites (Long Bridge, Short Bridge, Atop) on each of the three Cu facets [Cu(111), Cu(110), Cu(100)],

for a total of nine initial configurations.[50] Subsequent geometry optimizations of the Short Bridge and Atop configurations all converged to the Long Bridge binding site, except for the Cu(100) Short Bridge configuration, thereby yielding the following four optimized binding motifs of 4-octyne on Cu: Cu(111) Long Bridge, Cu(110) Long Bridge, Cu(100) Long Bridge, and Cu(100) Short Bridge. Side and top views of these optimized binding motifs are graphically depicted in Figure 4(c), where the presence of nonplanar C≡C−C (and C−C≡C) bond angles surrounding the central alkyne moiety clearly illustrate that 4-octyne has undergone significant qualitative geometrical changes (i.e., $sp \rightarrow sp^2$ rehybridization) upon adsorption onto the Cu surfaces. From Table 1, one immediately sees that the corresponding ΔU^{DFT} values, −39.70 kcal-mol^{-1} [Cu(111) Long Bridge], −35.68 kcal-mol^{-1} [Cu(110) Long Bridge], −42.06 kcal-mol^{-1} [Cu(100) Long Bridge], and −41.19 kcal-mol^{-1} [Cu(100) Short Bridge], are indeed substantially more favorable than those on SiO$_2$, and are consistent with chemisorption of 4-octyne onto this metallic surface. With a mean value of $\Delta U^{DFT} = -39.66 \pm 2.83$ kcal-mol^{-1}, the adsorption of 4-octyne on Cu is *approximately 26 kcal-mol^{-1} more favorable* than adsorption on SiO$_2$. As such, these binding energetics provide strong theoretical evidence that this coadsorbate molecule would form a strongly bound monolayer on Cu, which in turn could serve as a molecular blocking layer to thin-film growth on this surface.

Consistent with the literature precedent regarding the adsorption of small alkynes on Cu surfaces,[49] we find that the chemical origin of this differential binding energy is indeed a significant rehybridization ($sp \rightarrow sp^2$) of the triple bond in 4-octyne upon adsorption onto the Cu (and not the SiO$_2$) surfaces. As depicted in Table 1, this rehybridization is quite evident when considering the changes in the C≡C bond length and C−C≡C (and C≡C−C) bond angles in the adsorbed 4-octyne molecule. As a reference, the C≡C bond length and C−C≡C (or C≡C−C) bond angles are 1.21 Å and 178.8°, respectively, in the isolated (vapor-phase) 4-octyne molecule; these values are consistent with those found in alkynes like acetylene, which has a C≡C bond length of 1.21 Å and a H−C≡C (or C≡C−H) bond angle of 180.0°. Upon adsorption onto the high-symmetry/low-index facets of Cu, we find that the C≡C bond length in 4-octyne increases by ∼14% to 1.38 ± 0.01 Å, a value which sits between the C=C double bond lengths in ethylene (∼ 1.34 Å) and benzene (∼ 1.40 Å). In the same breath, the C−C≡C (and C≡C−C) bond angles in 4-octyne decrease by ∼30% to 124.9 ± 1.6°, a value which is very similar to the ideal C−C=C (or C=C−C) double bond angle of 120.0° found in an internal sp^2 hybridized carbon. Taken together, these geometric changes strongly indicate that 4-octyne has undergone a $sp \rightarrow sp^2$ rehybridization upon chemisorption onto the Cu surface, and provide further support for the substantially more favorable interaction (beyond nonbonded vdW/dispersion forces) between the coadsorbate and the underlying metal surface.

As discussed above in the *Theoretical Expectations*, a simple Langmuir adsorption model for the reversible and differential binding of the coadsorbate onto the dielectric and metal surfaces demonstrates that the substrate temperature (T_s) and coadsorbate partial pressure (p_A) are the two key process variables governing selective growth in our approach. As such, we have also considered how temperature and pressure effects will influence the adsorption of 4-octyne onto the SiO$_2$ and Cu surfaces by computing binding enthalpies $[\Delta H(T, p)]$ and binding Gibbs free energies $[\Delta G(T, p)]$ corresponding to the experimental conditions of $T = T_s = 120$ °C and $p = p_A = 0.36$ Torr (see the *Binding Energetics* section in the SI for more details). As depicted in Table 1, we find that the mean $\Delta H(T, p)$ values of −12.89 kcal-mol^{-1} (SiO$_2$) and −40.48 kcal-mol^{-1} (Cu) are both within 1.0 kcal-mol^{-1} of the ΔU^{DFT} values described above. Enthalpically speaking, we therefore find that the adsorption of 4-octyne onto Cu is ∼28 kcal-mol^{-1} more favorable than adsorption on SiO$_2$ at these finite T and p values. Even when accounting for entropic effects (which substantially disfavor surface adsorption), we find that 4-octyne still remains favorably *bound* to the Cu surface (with a mean exergonic value of $\Delta G = -8.12$ kcal-mol^{-1}), but is now *unbound* on the SiO$_2$ surface (with a mean endergonic value of $\Delta G = +14.48$ kcal-mol^{-1}). As such, these finite T and p binding energetics provide even stronger theoretical evidence that 4-octyne would form a strongly bound (yet reversible) monolayer on the Cu, which in turn could serve as a molecular blocking layer that will inhibit thin-film growth on this metal surface.

Growth of ZrO$_2$ Thin Films on Cu and SiO$_2$. To examine the effect of a coadsorbate species on the growth of ZrO$_2$ thin films in a CVD process, we have used the following experimental sequence (cf. Figure 1). First, after loading the substrates on the sample manipulator and inserting them into the intermediate UHV chamber, the samples were annealed at a temperature of 180 °C for an hour (with the curtain gas flowing and the reactor pressure set to 1.5 Torr). Using our ability to conduct in situ XPS without air-break, we found that this procedure is essential for producing a starting Cu surface devoid of oxides, possessing at most submonolayer coverages of adsorbed oxygen atoms. Next, the microreactor probe is placed in position for exposure of the substrates to the reactant streams. After the desired substrate temperature is achieved under the flow of pure carrier gases, the reactant streams are introduced sequentially. First, the coadsorbate 4-octyne is introduced for a time period of 30 s. Next the thin-film precursor (TEMAZ) is introduced for a time period of 2 min, while the 4-octyne continues to flow. Finally, the O$_2$ is introduced for a variable time period. The sequence is then reversed—after the O$_2$ flow is extinguished, TEMAZ continues to flow for 25 s before it is extinguished, and then the 4-octyne continues to flow for an additional time period of 30 s. The coadsorbate is "pre-dosed" to allow it to build up a steady-state coverage before introducing either the thin-film precursor or coreactant, as displayed above in Figure 1, thereby maximizing the effects of competitive adsorption on the selectivity.

First, we find that growth of a ZrO$_2$ thin film in the absence of the coadsorbate is essentially the same on SiO$_2$ and Cu—i.e., the deposition proceeds with no detectable incubation period, and the film thickness grows linearly with time. In Figure 5(a), we plot the thickness of the ZrO$_2$ thin film as a function of the duration of the O$_2$ pulse for growth on both SiO$_2$ and Cu in the presence of 4-octyne. Here the substrate temperature was $T_s = 120$ °C and the partial pressure of 4-octyne was $p_A = 0.36$ Torr. For growth on SiO$_2$, the thin-film thickness was assessed using in situ XPS and ex situ SE, while for growth on Cu it was assessed using in situ XPS (see Table S-1 in the SI for thin-film thickness values). We also display error bars for the thin-film thicknesses derived from repeated experiments and experimental uncertainties associated with the analytical techniques (SE and XPS). When the error bars are not visible, the uncertainties are smaller than the plot symbols.
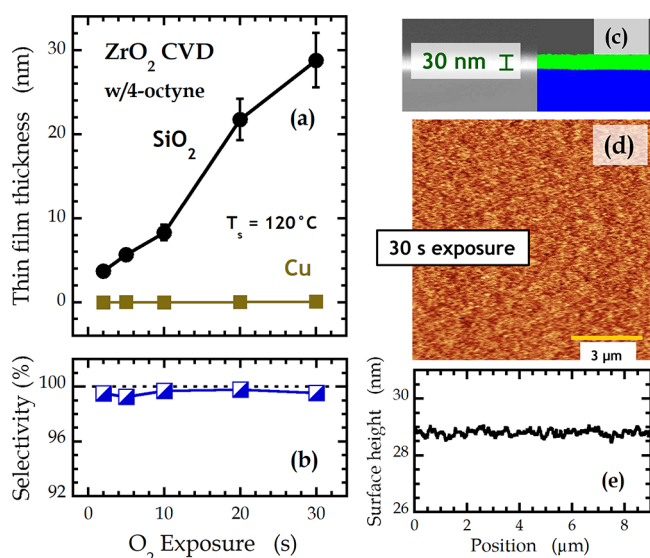
Figure 5. (a) Thin-film thickness of ZrO$_2$ as measured by ex situ spectroscopic ellipsometry (SE on SiO$_2$) and XPS (on Cu) as a function of the reaction time, determined by the O$_2$ exposure time {codosed with Zr[N(CH$_3$C$_2$H$_5$)]$_4$ and the coadsorbate 4-octyne}. The partial pressure of the coadsorbate (4-octyne) was p_A = 0.36 Torr and the substrate temperature was T_s = 120 °C. (b) The selectivity, computed using $S_{ASD} = (D_{gs} - D_{ns})/(D_{gs} + D_{ns})$, where D_{gs} (D_{ns}) is the thin-film thickness deposited on the growth (nongrowth) surface. (c) Cross-sectional SEM of the thin film formed on SiO$_2$ for an O$_2$ exposure of 30 s. The false color (green) region represents the thin film. (d) AFM image and (e) line scan of the thin film formed on SiO$_2$ for an O$_2$ exposure of 30 s. The latter has been scaled to the thin-film thickness measured by SE.

As may be seen, we observe essentially linear growth of ZrO$_2$ on SiO$_2$ (0.95 ± 0.08 nm-s^{-1}), while growth on Cu is virtually nonexistent. For example, less than a monolayer was observed on the Cu surface for all O$_2$ exposure times considered herein (i.e., most are <0.1 ML or 0.03 nm, after 30 s exposure we find ~0.3 ML or 0.07 nm). Using a formalism essentially equivalent to that introduced by Gladfelter,[6] we have also computed the selectivity of this approach via $S_{ASD} = (D_{gs} - D_{ns})/(D_{gs} + D_{ns})$, in which D_{gs} and D_{ns} are the thin-film thicknesses deposited on the growth and nongrowth surfaces, respectively. Thus, S_{ASD} is a quantity that will vary from 0 (no selectivity) to 1 (perfect selectivity). As may be seen in Figure 5(b), we find that the selectivity S_{ASD} > 0.99 (i.e., > 99%) in all of our experiments (with uncertainties that are all smaller than the plot symbols).

We have also examined selected ZrO$_2$ thin films deposited on SiO$_2$ using ex situ scanning electron microscopy (SEM) and AFM, with representative results shown in Figure 5(c,d). From a cleaved (i.e., scribed and diced) sample (30 s exposure), the cross-sectional SEM displayed in Figure 5(c) shows a ZrO$_2$ thin film that is smooth and uniform across the SiO$_2$ substrate, with a thickness (~ 30 nm) in close agreement with SE. In the SI, we also display larger (~ 1.1 μm and ~1.8 μm) scale cross sections, which also show a thin film that is uniform in thickness. From the AFM results, which are displayed in Figure 5(d) (10 × 10 μm^2 scan), we also observe a very smooth film [also see line scan in Figure 5(e)] with small granular features and a measured RMS roughness of ~0.1 nm. Importantly, we do not observe any detectable defects in the thin film, such as regions where the film is considerably different in thickness, or the substrate is exposed. In the SI, we provide examples of

substrates that possess pit/pinhole/vacancy defects, illustrating that AFM can detect defects of these types with diameters of ~0.02−0.07 μm. Defects of these sizes or larger are not observed here.

Given the results provided in Figure 5, which clearly demonstrate substrate-composition-dependent ASD, we now consider the effects of the process variables, the substrate temperature (T_s) and coadsorbate partial pressure (p_A). In order to do so, we conducted a series of experiments in which T_s was varied from 120 to 240 °C, and the partial pressure of 4-octyne was varied from 0.105 to 0.36 Torr at the substrate surface, while maintaining a constant partial pressure of TEMAZ (28 mTorr). In all cases, we used a 2 s exposure of O$_2$. In Figure 6, we present results from XPS for five different
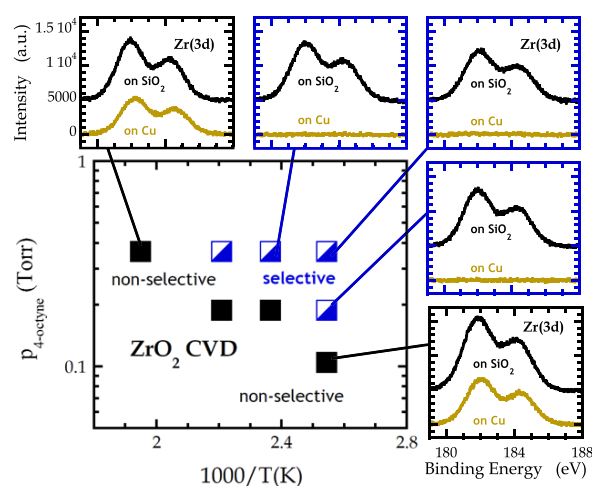

Figure 6. Main panel: Process phase space plotted in terms of the partial pressure of the coadsorbate (4-octyne) vs inverse substrate temperature. The half-filled squares represent conditions where we observed area-selective growth, i.e., deposition on SiO$_2$ but not Cu. The filled squares represent conditions where area-selective growth was not observed. In all cases, the O$_2$ exposure was 2 s. The five surrounding panels are the XP spectra acquired for the Zr(3d) region for both surfaces (SiO$_2$ and Cu), connected by tie lines to the process conditions used.

experiments, where we display the spectra for the Zr(3d) region observed on both SiO$_2$ and Cu. As may be seen from these spectra, we observe no growth on Cu and significant growth on SiO$_2$ for three of the five cases. Consideration of three additional sets of reaction conditions (XPS not shown) provided four overall sets of conditions that resulted in selectivity (indicated by symbol type/color). For the two extreme cases that we considered in Figure 6 (T_s = 120 °C, p_A ≈ 0.105 Torr; and T_s = 240 °C, p_A ≈ 0.36 Torr), we see that growth occurs on both SiO$_2$ and Cu. These results are entirely consistent with the theoretical expectations described in connection with Figure 3—both increasing the substrate temperature and reducing the partial pressure of 4-octyne will reduce the coverage of the coadsorbate on the Cu surface.

Although the results displayed in Figure 6 indicate that 4-octyne binds strongly to Cu and blocks growth on that surface, these findings alone cannot prove whether the chemisorption of 4-octyne is reversible or irreversible under these reaction conditions. To further examine this point, we completed the following experiment. Similar to the experiments described above, we begin by pre-exposing the SiO$_2$ and Cu substrates to

4-octyne (cf. Figure 1). In this case, we employed identical conditions to that used to obtain the results shown in Figure 5 (i.e., T_s = 120 °C and p_A = 0.36 Torr). After 30 s, the flow of 4-octyne was extinguished. Next, pure carrier gas was flowed to purge any remaining 4-octyne (30 s), which was followed by initiation of a flow of TEMAZ. After 2 min had elapsed, a 2 s pulse of O_2 was introduced. Finally, the flow of TEMAZ was continued for an additional 25 s, before all reactant flows were extinguished. We plot the results of this experiment in Figure 7
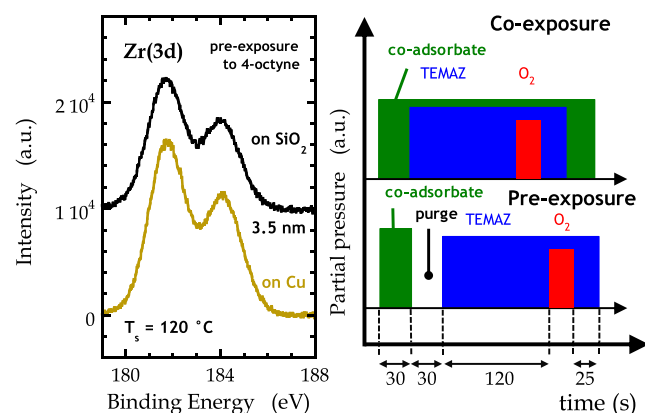

Figure 7. Left panel: XP spectra for the Zr(3d) region for an experiment where the coadsorbate was only pre-exposed to the two surfaces, before CVD using $Zr[N(CH_3C_2H_5)]_4$ and O_2. The O_2 exposure was 2 s. The XP spectra measured on SiO_2 has been shifted along the ordinate for clarity. Right panel: Exposure sequences used for the coexposure (see Figures 5 and 6) and pre-exposure experiments. The height of the bars for each species does not represent relative partial pressures.

for the Zr(3d) feature on both SiO_2 and Cu. From XPS, we observe strong intensity on both surfaces, and analysis via SE indicates the formation of ~3.5 nm thick ZrO_2 thin film on SiO_2. In the presence of a 4-octyne coexposure (cf. Figures 5 and 6), we observed a thin film with a similar thickness on SiO_2 (~ 3.8 nm from SE). Hence, the clear conclusion of this experiment is that the residence time of 4-octyne on Cu for these reaction conditions (T_s = 120 °C) is too short to affect the desired blocking of growth of the ZrO_2 thin film, and chemisorption is reversible under these experimental conditions and time scales.

Next, we consider the composition of the deposited thin films. First, all XPS measurements were conducted with no additional treatment of the substrates (e.g., high-temperature annealing, sputtering, etc.). Given the use of 4-octyne as the coadsorbate, it was reasonable to expect the build-up of a C-containing contamination layer on the substrates following reaction and cooling to room temperature for subsequent analysis using XPS (typically acquired several hours after the reaction), and indeed this was the case. Angle-resolved XPS (ARXPS) revealed the formation of a contamination layer on essentially all substrates, and subsequent analysis implicated that these layers were typically a few Å in thickness, approaching ~10 Å in a few cases. In the SI, we present results for the C(1s) intensity obtained in connection with the results shown in Figure 6 and find no correlation between this intensity and whether or not selectivity is achieved. Finally, we also found evidence for C−O bonds in these layers. As a consequence, to assess the composition of the Zr-containing thin film, we will focus on the binding energies observed for

the Zr(3d) and O(1s) features. That is, we will not attempt an estimate of the stoichiometry using the absolute intensities of these features, their photoelectron cross sections, and attenuation effects that vary with photoelectron kinetic energy.

In Figure 8, we plot the binding energy found for the Zr(3d) and O(1s) peaks for the thin films considered in Figure 5. In
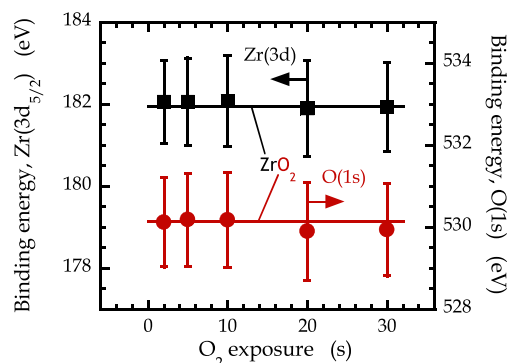
Figure 8. Binding energy for the $Zr(3d_{5/2})$ and O(1s) peaks found from in situ XPS of the thin films deposited on SiO_2 as a function of O_2 exposure. These are the same thin films that were considered in Figure 5 above. The errors bars represent the fwhm's found from fits to the spectra, while the horizontal lines represent the binding energies reported in a previous study of ZrO_2 thin films (ref 51).

all cases, the spectra were normalized by using the binding energy for adventitious C(1s) of 284.6 eV. The errors bars represent the fwhm found from fits to the data. We also plot as horizontal lines the binding energy observed for these two peaks for stoichiometric thin films of ZrO_2 (plasma-deposited and postdeposition annealed) reported by Lucovsky and co-workers,[51] namely 181.94 eV for Zr(3d) and 530.13 eV for O(1s). As may be seen, we observe binding energies consistent with the formation of essentially stoichiometric ZrO_2 in all cases.

■ DISCUSSION

In this work, we have presented results that unequivocally demonstrate that the addition of 4-octyne to a CVD process based on the reaction of $Zr[N(CH_3C_2H_5)]_4$ (TEMAZ) and O_2 results in substrate-composition-dependent growth of ZrO_2 on SiO_2 but not Cu. As we indicated in the Introduction, substrate-composition dependence is necessary for self-aligned ASD, which is arguably the most important ASD application. We find that growth is selective over a wide range of conditions, including substrate temperatures of T_s = 120−180 °C. DFT calculations indicate that the binding of 4-octyne to the Cu surface is substantial due to a $sp \rightarrow sp^2$ rehybridization of the internal alkyne moiety in the coadsorbate molecule. In stark contrast, the binding of this coadsorbate molecule on an amorphous hydroxyl-terminated SiO_2 surface is much weaker, and consistent with physisorption due to vdW/dispersion interactions alone. Reducing the partial pressure of 4-octyne or raising the substrate temperature sufficiently results in a loss of selectivity; this is consistent with a mechanism that involves competitive adsorption where chemisorbed 4-octyne blocks sites for the chemisorption of TEMAZ (and possibly O_2). From XPS, we find binding energies for Zr(3d) and O(1s) that are in agreement with the formation of stoichiometric ZrO_2, while significant incorporation of C into the thin film is not observed. The thin films are smooth (with a RMS roughness of

~0.1 nm for a thin-film thickness of ~30 nm) and continuous. In the SI, we present a result where we demonstrate ASD on a patterned substrate with 50 μm features. Although a test of our ASD process at the ~10 nm scale is certainly of interest (where issues such as diffusion, overgrowth, and feature edge effects can be important), this was not the focus of the current work. At minimum, the selective process we have described here is arguably fast from an industrial perspective (i.e., 30 nm of thin film in 30 s) and involves all vapor-phase species, including a coadsorbate which only consists of C and H. Finally, other than the presence of a near surface C-containing contamination layer, the Cu surface was relatively untouched.

Placing our work in context, the previous studies that are most similar to ours are (i) the work by Mackus, Kessels, and co-workers reporting the "ABC" method of ALD,[25] and (ii) the use of a molecular inhibitor by Abelson and co-workers.[26,27] Concerning the first, the ABC method does involve the use of a third chemical species to bind selectively to one surface over another to block sites for growth. Since it is ALD, the possible complications caused by unwanted side reactions with the thin-film precursor or the coreactant are eliminated. As such, it should be "easier" in theory to select the blocking species since these side reactions need not be considered. For this approach to work, however, chemisorption of the blocking species must be effectively irreversible (based on the time scale of the ALD process). As we have shown with the data displayed in Figure 7, our process likely does not involve irreversible chemisorption as a predose of 4-octyne was insufficient to block growth of ZrO_2 on Cu. In other words, only when 4-octyne was codosed do we achieve selectivity. Finally, although elegantly executed, the ABC process could only deposit about ~1.5 nm of a thin film on the desired growth surface, before growth commenced on the nongrowth surface, which significantly limits the applications of the specific system studied.

Concerning the second set of studies,[26,27] as we indicated in the Introduction, this work involved the use of "single-source" thin-film precursors and a molecular inhibitor (similar to our use of a coadsorbate). Most importantly, however, there was no coreactant in this work. In one case, vinyl trimethylsilane (VTMS) was used in combination with a Cu thin-film precursor possessing VTMS as a ligand, possibly to induce reversible adsorption. This system showed high intrinsic selectivity (e.g., significant growth on RuO_2 vs much smaller growth on SiO_2), which could be increased by the introduction of VTMS, although growth was suppressed to a certain extent on all surfaces. In another study, NH_3 was examined as a molecular inhibitor concerning the decomposition of transition metal (Mo, Fe, Ru) carbonyls on a variety of surfaces. Decomposition could be inhibited on a number of oxide surfaces by NH_3, but the exact mechanism could not be identified. In addition, significant incorporation of N was also observed, which suggests that the inhibitor acted as a coreactant.

Returning to the work we have presented here, the interpretation of our results is straightforward. The coadsorbate 4-octyne chemisorbs strongly (but reversibly) on the Cu surface and prevents dissociative chemisorption of the thin-film precursor. Chemisorption of the coreactant O_2 may also be suppressed by chemisorbed 4-octyne. For the conditions examined in this work, chemisorption is not sufficiently strong such that pre-exposure of the substrate to 4-octyne can effectively block growth for an extended period of time based

on the experiment shown in Figure 7. We concede that the possibility exists that 4-octyne could be present on the Cu surface at the beginning of the O_2 dose, but is removed by reaction with the impinging O_2. In the absence of a codose of 4-octyne in the vapor phase, however, this adsorbed layer of 4-octyne cannot be reformed. In any event, coexposure of 4-octyne is required to produce the desired selectivity in our case.

How generic is our approach to achieving ASD by employing an appropriately chosen coadsorbate? In principle, this approach should be widely applicable, provided that suitable chemical bonding interactions (and lack thereof) can be identified concerning the targeted surfaces. In our case, we considered a Group 11 transition metal, Cu, which tends not to form particularly strong covalent bonds due to its filled d-electron shell (it is also not particularly reactive in comparison to the Group 8−10 transition metals, many of which are well-known for their catalytic activity). Due to a $sp \rightarrow sp^2$ rehybridization of the 4-octyne, this molecule binds strongly to Cu surfaces, making it a good choice as a coadsorbate to block chemisorption of other species. If one were to consider other transition metal surfaces, then one can easily imagine a wide variety of relatively small molecules that could bind strongly and act as effective molecular blocking agents. For many oxides, including SiO_2, the presence of terminating species determines reactivity with thin-film precursors. In our case, a ligand exchange reaction with $-OH(a)$ species {which could produce, for example, $HN(CH_3C_2H_5)(g)$, and $-O-Zr[N(CH_3C_2H_5)]_3(a)$}, represents the first step to nucleating a ZrO_2 thin film. Here, for our conditions, 4-octyne does not chemically bind to $-OH(a)$, and exhibits only weak vdW/dispersion interactions with the dielectric surface. Again, one could imagine a variety of species that will also weakly interact with these surface hydroxyl species.

Could this approach work for the inverse case, i.e., achieving selective growth on Cu (or some other metal) while blocking growth on SiO_2 (or some other dielectric)? In this case, there is no reason to expect that one could not identify a suitable family of chemical species that would bind preferentially to SiO_2 vs Cu. As discussed in the Introduction, a number of previous studies have investigated the use of molecules that form SAMs on SiO_2, binding strongly to $-OH(a)$ species.[8,9,22,23] We have reported,[23] for example, that vapor-phase delivery of alkyl silanes can selectively hinder ALD growth of TaN_x thin films on SiO_2, while not affecting their growth on Cu. In this case, these blocking layers were formed once, before growth, and coexposure was not investigated. Using the approach developed in this work, direct reactions between the coadsorbate and the thin-film precursor would have to be considered (and minimized) to make this strategy viable.

Finally, could this approach work for ALD? In this case, one would preferably introduce the coadsorbate in the half cycle when the thin-film precursor is introduced. Chemisorption of the precursor would be blocked by an appropriately chosen coadsorbate molecule that binds strongly to the targeted nongrowth surface and does not directly react with the precursor. In this approach, potentially unwanted interactions between the coadsorbate and coreactant (including plasmas) need not be considered. As such, one could argue that the implementation of our scheme should be easier concerning ALD vis-à-vis CVD.

CONCLUSIONS

In this work, we have presented experimental and theoretical results describing an approach to substrate-composition-dependent deposition that employs a coadsorbate which binds selectively to one surface (a metal, Cu) over another (a dielectric, SiO_2). The selective dielectric-on-dielectric (DoD) process developed herein has obvious applications in area-selective deposition (ASD), is fast, completely vapor phase, and does not negatively change the composition (or morphology) of the deposited thin film. The process phase space for selective growth follows expectations for a mechanism involving competitive adsorption—selectivity is lost at sufficiently high substrate temperatures or sufficiently small coadsorbate partial pressures. The thin films that were deposited on the targeted growth surface are of a composition expected for an unaltered CVD process, and are smooth (roughness is of atomic dimensions) and continuous. In general, we anticipate that this approach should work for a variety of systems involving combinations of metals, semiconductors, and dielectrics, providing that suitable chemical interactions can be identified.

ASSOCIATED CONTENT

Ⓢ Supporting Information

The Supporting Information is available free of charge at https://pubs.acs.org/doi/10.1021/acsami.9b22065.

> Computational details regarding the binding energetics, XPS analysis of the C(1s) peak, SEMs of a ZrO_2 thin film on SiO_2, examples of AFM images where thin-film defects can be identified, and results from ARXPS and scanning Auger microscopy of a thin film deposited on a patterned wafer (PDF)

AUTHOR INFORMATION

Corresponding Authors

Robert A. DiStasio, Jr. − *Department of Chemistry and Chemical Biology, Cornell University, Ithaca, New York 14853, United States;* ⓞ orcid.org/0000-0003-2732-194X; Email: distasio@cornell.edu

James R. Engstrom − *Robert F. Smith School of Chemical and Biomolecular Engineering, Cornell University, Ithaca, New York 14853, United States;* ⓞ orcid.org/0000-0001-8505-8188; Email: jre7@cornell.edu

Authors

Taewon Suh − *Robert F. Smith School of Chemical and Biomolecular Engineering, Cornell University, Ithaca, New York 14853, United States;* ⓞ orcid.org/0000-0001-6382-3811

Yan Yang − *Department of Chemistry and Chemical Biology, Cornell University, Ithaca, New York 14853, United States*

Pengyuan Zhao − *Robert F. Smith School of Chemical and Biomolecular Engineering, Cornell University, Ithaca, New York 14853, United States*

Ka Un Lao − *Department of Chemistry and Chemical Biology, Cornell University, Ithaca, New York 14853, United States;* ⓞ orcid.org/0000-0002-3993-536X

Hsin-Yu Ko − *Department of Chemistry and Chemical Biology, Cornell University, Ithaca, New York 14853, United States;* ⓞ orcid.org/0000-0003-1619-6514

Jonathan Wong − *Department of Chemistry and Chemical Biology, Cornell University, Ithaca, New York 14853, United States*

Complete contact information is available at:
https://pubs.acs.org/10.1021/acsami.9b22065

Notes

The authors declare no competing financial interest.

ACKNOWLEDGMENTS

REFERENCES

(1) Engstrom, J. R.; Kummel, A. C. Preface: Special Topic on Atomic and Molecular Layer Processing: Deposition, Patterning, and Etching. *J. Chem. Phys.* **2017**, *146* (5), 052501.

(2) Clark, R.; Tapily, K.; Yu, K.-H.; Hakamata, T.; Consiglio, S.; O'Meara, D.; Wajda, C.; Smith, J.; Leusink, G. Perspective: New Process Technologies Required for Future Devices and Scaling. *APL Mater.* **2018**, *6* (5), 058203.

(3) Carlsson, J. O. Selective Vapor-Phase Deposition on Patterned Substrates. *Crit. Rev. Solid State Mater. Sci.* **1990**, *16* (3), 161−212.

(4) Kuech, T. F.; Goorsky, M. S.; Tischler, M. A.; Palevski, A.; Solomon, P.; Potemski, R.; Tsai, C. S.; Lebens, J. A.; Vahala, K. J. Selective Epitaxy of GaAs, $Al_xGa_{1-x}As$ and $In_xGa_{1-x}As$. *J. Cryst. Growth* **1991**, *107* (1-4), 116−128.

(5) Bhat, R. Current Status of Selective Area Epitaxy by OMCVD. *J. Cryst. Growth* **1992**, *120*, 362−368.

(6) Gladfelter, W. L. Selective Metallization by Chemical Vapor Deposition. *Chem. Mater.* **1993**, *5*, 1372−1388.

(7) Hampden-Smith; Kodas, T. T. Chemical Vapor Deposition of Metals: Part 2. Overview of Selective CVD of Metals. *Chem. Vap. Deposition* **1995**, *1* (2), 39−48.

(8) Yan, M.; Koide, Y.; Babcock, J. R.; Markworth, P. R.; Belot, J. A.; Marks, T. J.; Chang, R. P. H. Selective-Area Atomic Layer Epitaxy Growth of ZnO Features on Soft Lithography-Patterned Substrates. *Appl. Phys. Lett.* **2001**, *79* (11), 1709−1711.

(9) Jiang, X.; Bent, S. F. Area-Selective ALD with Soft Lithographic Methods: Using Self-Assembled Monolayers to Direct Film Deposition. *J. Phys. Chem. C* **2009**, *113*, 17613−17625.

(10) Mackus, A. J. M.; Bol, A. A.; Kessels, W. M. M. The Use of Atomic Layer Deposition in Advanced Nanopatterning. *Nanoscale* **2014**, *6*, 10941−10960.

(11) Fang, M.; Ho, J. C. Area-Selective Atomic Layer Deposition: Conformal Coating, Subnanometer Thickness Control, and Smart Positioning. *ACS Nano* **2015**, *9* (9), 8651−8654.

(12) Mackus, A. J. M.; Merkx, M. J. M; Kessels, W. M. M. From the Bottom-Up: Toward Area-Selective Atomic Layer Deposition with High Selectivity. *Chem. Mater.* **2019**, *31*, 2−12.

(13) George, S. M. Atomic Layer Deposition: An Overview. *Chem. Rev.* **2010**, *110*, 111−131.

(14) Leskela, M.; Ritala, M. Atomic Layer Deposition Chemistry: Recent Developments and Future Challenges. *Angew. Chem., Int. Ed.* **2003**, *42* (45), 5548−5554.

(15) Puurunen, R. L. Surface Chemistry of Atomic Layer Deposition: A Case Study for the Trimethylaluminum/Water Process. *J. Appl. Phys.* **2005**, *97* (12), 121301.

(16) Green, M. L.; Ho, M.-Y.; Busch, B.; Wilk, G. D.; Sorsch, T.; Conard, T.; Brijs, B.; Vandervorst, W.; Räisänen, P. I.; Muller, D.; Bude, M.; Grazul, J. Nucleation and Growth of Atomic Layer Deposited HfO$_2$Gate Dielectric Layers on Chemical Oxide (Si-O-H) and Thermal Oxide (SiO$_2$ or Si-O-N) Underlayers. *J. Appl. Phys.* **2002**, *92* (12), 7168−7174.

(17) McDonnell, S.; Longo, R. C.; Seitz, O.; Ballard, J. B.; Mordi, G.; Dick, D.; Owen, J. H. G.; Randall, J. N.; Kim, J.; Chabal, Y. J.; Cho, K.; Wallace, R. M. Controlling the Atomic Layer Deposition of Titanium Dioxide on Silicon: Dependence on Surface Termination. *J. Phys. Chem. C* **2013**, *117*, 20250−20259.

(18) Hughes, K. J.; Engstrom, J. R. Nucleation Delay in Atomic Layer Deposition on a Thin Organic Layer and the Role of Reaction Thermochemistry. *J. Vac. Sci. Technol., A* **2012**, *30* (1), 01A102.

(19) Vallat, R.; Gassilloud, R.; Eychenne, B.; Vallée, C. Selective Deposition of Ta$_2$O$_5$ by Adding Plasma Etching Super-Cycles in Plasma Enhanced Atomic Layer Deposition Steps. *J. Vac. Sci. Technol., A* **2017**, *35* (1), 01B104.

(20) Vos, M. F. J.; Chopra, S. N.; Verheijen, M. A.; Ekerdt, J. G.; Agarwal, S.; Kessels, W. M. M.; Mackus, A. J. M. Area-Selective Deposition of Ruthenium by Combining Atomic Layer Deposition and Selective Etching. *Chem. Mater.* **2019**, *31* (11), 3878−3882.

(21) Song, S. K.; Saare, H.; Parsons, G. N. Integrated Isothermal Atomic Layer Deposition/Atomic Layer Etching Supercycles for Area-Selective Deposition of TiO$_2$. *Chem. Mater.* **2019**, *31* (13), 4793−4804.

(22) Park, K. J.; Doub, J. M.; Gougousi, T.; Parsons, G. N. Microcontact Patterning of Ruthenium Gate Electrodes by Selective Area Atomic Layer Deposition. *Appl. Phys. Lett.* **2005**, *86* (5), 051903.

(23) Zhang, W.; Engstrom, J. R. Effect of Substrate Composition on Atomic Layer Deposition Using Self-Assembled Monolayers as Blocking Layers. *J. Vac. Sci. Technol., A* **2016**, *34* (1), 01A107.

(24) Chopra, S. N.; Zhang, Z.; Kaihlanen, C.; Ekerdt, J. G. Selective Growth of Titanium Nitride on HfO$_2$ across Nanolines and Nanopillars. *Chem. Mater.* **2016**, *28*, 4928−4934.

(25) Mameli, A.; Merkx, M. J. M.; Karasulu, B.; Roozeboom, F.; Kessels, W. M. M.; Mackus, A. J. M. Area-Selective Atomic Layer Deposition of SiO$_2$ Using Acetylacetone as a Chemoselective Inhibitor in an ABC-Type Cycle. *ACS Nano* **2017**, *11* (9), 9303−9311.

(26) Babar, S.; Mohimi, E.; Trinh, B.; Girolami, G. S.; Abelson, J. R. Surface-Selective Chemical Vapor Deposition of Copper Films through the Use of a Molecular Inhibitor. *ECS J. Solid State Sci. Technol.* **2015**, *4* (7), N60−N63.

(27) Mohimi, E.; Zhang, Z. V.; Liu, S.; Mallek, J. L.; Girolami, G. S.; Abelson, J. R. Area Selective CVD of Metallic Films from Molybdenum, Iron, and Ruthenium Carbonyl Precursors: Use of Ammonia to Inhibit Nucleation on Oxide Surfaces. *J. Vac. Sci. Technol., A* **2018**, *36* (4), 041507.

(28) Langmuir, I. The Mechanism of the Catalytic Action of Platinum in the Reactions 2CO + O$_2$ = 2CO$_2$ and 2H$_2$ + O$_2$ = H$_2$O. *Trans. Faraday Soc.* **1922**, *17*, 621−654.

(29) Roadman, S. E.; Maity, N.; Carter, J. E.; Engstrom, J. R. Study of Thin Film Deposition Processes Employing Variable Kinetic Energy, Highly Collimated Neutral Molecular Beams. *J. Vac. Sci. Technol., A* **1998**, *16* (6), 3423−3433.

(30) Hughes, K. J.; Engstrom, J. R. Nucleation Delay in Atomic Layer Deposition on a Thin Organic Layer and the Role of Reaction Thermochemistry. *J. Vac. Sci. Technol., A* **2012**, *30* (1), 01A102.

(31) Zhang, W.; Nahm, R. K.; Ma, P. F.; Engstrom, J. R. Probing Ultrathin Film Continuity and Interface Abruptness with X-ray Photoelectron Spectroscopy and Low-Energy Ion Scattering. *J. Vac. Sci. Technol., A* **2013**, *31* (6), 061101.

(32) Chen, J.-R.; Zhang, W.; Nahm, R. K.; DiFeo, M. A.; Engstrom, J. R. Design and Characterization of a Microreactor for Spatially

Confined Atomic Layer Deposition and in Situ UHV Surface Analysis. *J. Vac. Sci. Technol., A* **2017**, *35* (6), 061604.

(33) Giannozzi, P.; Andreussi, O.; Brumme, T.; Bunau, O.; Nardelli, M. B.; Calandra, M.; Car, R.; Cavazzoni, C.; Ceresoli, D.; Cococcioni, M.; et al. Advanced Capabilities for Materials Modelling with Quantum ESPRESSO. *J. Phys.: Condens. Matter* **2017**, *29* (46), 465901.

(34) Perdew, J. P.; Burke, K.; Ernzerhof, M. Generalized Gradient Approximation Made Simple. *Phys. Rev. Lett.* **1996**, *77* (18), 3865−3868.

(35) Ferri, N.; DiStasio, R. A., Jr.; Ambrosetti, A.; Car, R.; Tkatchenko, A. Electronic Properties of Molecules and Surfaces with a Self-Consistent Interatomic van der Waals Density Functional. *Phys. Rev. Lett.* **2015**, *114* (17), 176802/1−5.

(36) Tkatchenko, A.; Scheffler, M. Accurate Molecular van der Waals Interactions from Ground-State Electron Density and Free-Atom Reference Data. *Phys. Rev. Lett.* **2009**, *102* (7), 073005/1−4.

(37) Ruiz, V. G.; Liu, W.; Zojer, E.; Scheffler, M.; Tkatchenko, A. Density-Functional Theory with Screened van der Waals Interactions for the Modeling of Hybrid Inorganic-Organic Systems. *Phys. Rev. Lett.* **2012**, *108* (14), 146103/1−5.

(38) Xie, S.; Tu, L.; Han, Y.; Huang, L.; Kang, K.; Lao, K. U.; Poddar, P.; Park, C.; Muller, D. A.; DiStasio, R. A., Jr.; Park, J. Coherent, Atomically Thin Transition-Metal Dichalcogenide Super-lattices with Engineered Strain. *Science* **2018**, *359* (6380), 1131−1136.

(39) Hamann, D. R.; Schlüter, M.; Chiang, C. Norm-Conserving Pseudopotentials. *Phys. Rev. Lett.* **1979**, *43* (20), 1494−1497.

(40) Vanderbilt, D. Optimally Smooth Norm-Conserving Pseudo-potentials. *Phys. Rev. B.* **1985**, *32* (12), 8412−8415.

(41) Hamann, D. R. Optimized Norm-Conserving Vanderbilt Pseudopotentials. *Phys. Rev. B.* **2013**, *88* (8), 085117/1−10.

(42) Monkhorst, H. J.; Pack, J. D. Special Points for Brillouin-Zone Integrations. *Phys. Rev. B* **1976**, *13* (12), 5188−5192.

(43) Sandupatla, A. S.; Alexopoulos, K.; Reyniers, M. F.; Marin, G. B. DFT Investigation into Alumina ALD Growth Inhibition on Hydroxylated Amorphous Silica Surface. *J. Phys. Chem. C* **2015**, *119* (32), 18380−18388.

(44) Togo, A.; Tanaka, I. First Principles Phonon Calculations in Materials Science. *Scr. Mater.* **2015**, *108*, 1−5.

(45) Jerzy, L., Ed. *Handbook of Computational Chemistry*; Springer Science & Business Media, 2012 Chapter 10, 293−360.

(46) Elliott, S. D.; Dey, G.; Maimaiti, Y. Classification of Processes for the Atomic Layer Deposition of Metals Based on Mechanistic Information from Density Functional Theory Calculations. *J. Chem. Phys.* **2017**, *146* (5), 052822.

(47) Lifshitz, E. M., Hamermesh, M. The Theory of Molecular Attractive Forces between Solids. In *Perspectives in Theoretical Physics*; Pergamon, 1992, 329−349.

(48) Zaremba, E.; Kohn, W. Van der Waals Interaction between an Atom and a Solid Surface. *Phys. Rev. B* **1976**, *13* (6), 2270−2285.

(49) Bao, S.; Schindler, K.-M.; Hofmann, P.; Fritzsche, V.; Bradshaw, A. M.; Woodruff, D. P. The Local Adsorption Structure of Acetylene on Cu(111). *Surf. Sci.* **1993**, *291* (3), 295−308.

(50) Liu, W.; Lian, J. S.; Jiang, Q. Theoretical Study of C$_2$H$_2$ Adsorbed on Low-Index Cu Surfaces. *J. Phys. Chem. C* **2007**, *111* (49), 18189−18194.

(51) Rayner, G. B.; Kang, D.; Zhang, Y.; Lucovsky, G. Nonlinear Composition Dependence of X-ray Photoelectron Spectroscopy and Auger Electron Spectroscopy Features in Plasma-Deposited Zirconium Silicate Alloy Thin Films. *J. Vac. Sci. Technol., B: Microelectron. Process. Phenom.* **2002**, *20* (4), 1748−1758.